

This item was submitted to Loughborough's Institutional Repository (<https://dspace.lboro.ac.uk/>) by the author and is made available under the following Creative Commons Licence conditions.



CC creative commons
COMMONS DEED

Attribution-NonCommercial-NoDerivs 2.5

You are free:

- to copy, distribute, display, and perform the work

Under the following conditions:

 **Attribution.** You must attribute the work in the manner specified by the author or licensor.

 **Noncommercial.** You may not use this work for commercial purposes.

 **No Derivative Works.** You may not alter, transform, or build upon this work.

- For any reuse or distribution, you must make clear to others the license terms of this work.
- Any of these conditions can be waived if you get permission from the copyright holder.

Your fair use and other rights are in no way affected by the above.

This is a human-readable summary of the [Legal Code \(the full license\)](#).

[Disclaimer](#) 

For the full text of this licence, please go to:
<http://creativecommons.org/licenses/by-nc-nd/2.5/>

An experimental study of microneedle assisted micro-particle delivery

Dongwei Zhang, Diganta B Das*, Chris D Rielly

Department of Chemical Engineering, Loughborough University, Loughborough LE113TU,
Leicestershire. UK

Accepted for Publication in

Journal of Pharmaceutical Science

June 2013

(*Corresponding Author; Email: d.b.das@lboro.ac.uk)

An experimental study of microneedle assisted micro-particle delivery

Dongwei Zhang, Diganta B Das*, Chris D Rielly

Department of Chemical Engineering, Loughborough University, Loughborough LE113TU,
Leicestershire. UK

(*Corresponding Author; Email: d.b.das@lboro.ac.uk)

Abstract

A set of well defined experiments has been carried out to explore if microneedles (MNs) can enhance the penetration depths of micro-particles moving at high velocity such as those expected in gene guns for delivery of gene loaded micro-particles into target tissues. These experiments are based on applying solid MNs which are used to reduce the effect of mechanical barrier function of the target so as to allow delivery of micro-particles at less imposed pressure as compared to most typical gene guns. Further, a low cost material, namely, biomedical grade stainless steel micro-particle with size ranging between 1 - 20 μm , has been used in this study. The micro-particles are compressed and bound in the form of a cylindrical pellet and mounted on a ground slide, which are then accelerated together by compressed air through a barrel. When the ground slide reaches the end of the barrel, the pellet is separated from the ground slide and is broken down into particle form by a mesh that is placed at the end of the barrel. Subsequently, these particles penetrate into the target. This paper investigates the implications of velocity of the pellet along with various other important factors that affect the particle delivery into the target. Our results suggest that the particle passage increases with an increase in pressure, mesh pore size and decreases with increase in Polyvinylpyrrolidone (PVP) concentration. Most importantly, it is shown that MNs increase the penetration depths of the particles.

Key words: Gene gun, stainless steel, MN, micro-particles, penetration depth, passage percentage

1. Introduction

Micro-particle delivery systems (e.g., gene guns) have been used for transferring genes into cells and tissues (e.g. plant tissues) for some time.¹⁻⁶ Typically, the operation involves a micro-particle accelerator, which can deliver gene-loaded micro-particles into a target (e.g.

biological cells) to achieve the desired mass transfer effect (e.g. gene transfection). The PowderJect delivery system is a case in point, which has been applied to exploit the micro-particle gene transfer treatment.⁷⁻⁸ In most cases, these delivery systems are based on the principle that biocompatible micro-particles loaded with genes can be accelerated to a sufficient velocity so as to penetrate the barrier function of the target tissue and thereby achieve gene delivery.⁹⁻¹⁰ However, cell and tissue damages are particular problems for these micro-particle delivery systems which are discussed further later.

It is obvious from previous research on micro-particle based gene delivery that knowledge of the velocity of the micro-particles and its effects on particle penetration is one of the major research points in development of these systems. A number of researchers have studied the particle velocity for various designs of gene guns. For example, Quinlan et al.¹¹ have used a conical nozzle employed at 60 bar to accelerate polymeric micro-particles of 4.7, 15.5 and 26.1 μm diameters to velocities of 350, 460 and 465 m/s, respectively. Kendall et al.¹² have used a converging-diverging nozzle, which has been shown to accelerate polystyrene particles of diameter 4.7 μm to a velocity of 800 m/s at the same pressure as used by Quinlan et al.¹¹. Such developments of the delivery systems can improve the velocity of micro-particles to achieve a higher speed if compared with conical nozzles¹¹. Mitchell et al.¹³ have also studied the velocities of polystyrene particles (average size: 99 μm) for a light gas gun (LGG) proposed originally by Crozier¹⁴ and gold particles (average size: 3.03 μm) for a contoured shock tube (CST). The particle velocity is shown to achieve 170, 250 and 330 m/s at pressure of 20, 40 and 60 bar for the LGG, respectively. The gold particles have been shown to achieve an average velocity of 550 m/s at 60 bar based on the CST. Liu et al.¹⁵ have also used a CST to accelerate gold particles of diameter 2.7 μm to a velocity of 626 m/s at 60 bar pressure. Subsequently, Liu et al.¹⁶ used polystyrene particles of 39 ± 1 μm diameter to study the particle velocity for CST and found improvements relative to the LGG, which is shown to achieve a velocity of 570 ± 14.7 m/s at 60 bar pressure. In recent years, Soliman et al.¹⁷ have shown that a supersonic core jet can accelerate 1.8 and 5 μm diameters gold particles to velocities of 550 and 294 m/s at 30 bar pressure. O'Brien et al.⁵ have also used gold particles of core diameters 40 nm and 1 μm to achieve maximum depths of 31 ± 6 and 50 ± 11 μm in mouse ear tissue by using a Helios gene gun.

Although very high velocities of the micro-particles or/and gas may seem useful in delivering the particles deep into the target tissue, they may actually damage the target from their impacts. As such, it is logical that one controls both the velocity and, the mass of the micro-particles and gas that impact the target. This is somewhat reflected in a study by Belyantseva¹⁸ who has used a pressurized Helios gene gun to accelerate DNA-coated gold particles (1 μm diameter) where the pressure is controlled at 14 bar. The author shows that this pressure is adequate for the penetration of the particles without excessive tissue damage. Xia et al.¹⁹ have suggested that the pressure should be limited to around 14 bar to minimize damage for biolistic transfer to soft tissue. Uchida et al.²⁰ have fired plasmid DNA into cultured mammalian cells (e.g. human embryonic kidney cell (HEK293) and human breast adenocarcinoma (MCF7) cell) using a Helios gene gun, which shows that gene transfection is achieved in these cells but the cell damage occurs if the operating pressure in the gene gun is more than 200 psi (13.78 bar). O'Brien et al.⁵ have cultured HEK293 cells and used them as targets for biolistic transfection using a gene gun. This work has shown that nanoparticles can be utilised as gene carriers similar to micro-particles for biolistic transfection and lessen cell damage. These researches⁵ show that cell damage can be reduced if particle size and operation pressure are reduced as they lower the particle impact force on the cells/tissue such as those observed by Uchida et al.²⁰. In most studies, the viable dermis layer of skin is considered as the target tissue for gene loaded micro-particle delivery as the penetration depth is limited by a number of factors.^{11,21}

In the particles delivery process, the material of the particles is also of crucial importance. In order to deliver gene loaded particles into cells effectively, high density materials are generally preferred since they carry a larger momentum and are expected to penetrate more into the target tissue as compared to particles of low density materials. The most common material of the particles is gold due to its high density, low toxicity and lack of chemical inactivity. However, gold is an expensive material. In principle, other materials such as biomedical grade stainless steel and polystyrene may be a good replacement for gold while reducing the cost due to the lower price of these materials in comparison to gold. However, these materials have lower density compared to gold and, as such, the momentum for these micro-particles would be less for the same particles size and velocity. This implies that other factor is needed to break the resistance of the target tissue for the particles to enter easily while also enhancing the penetration depths. Microneedles (MNs), which can break the

resistance of the target tissue almost painlessly,²²⁻²⁶ seem to be a promising option in this regards. However, there is little or no study at the moment that demonstrates that MNs can be useful in the delivery of dry particulates particularly at lower pressures as compared to most current gene guns which should be operated at very high pressure.^{11,13,16} Previously, several studies have shown that the effectiveness of the MN based drug delivery is limited by a wide varieties of variables, e.g. MN height, spaces between the needles, patch size, insertion forces, tissue characteristics such as viscoelastic properties, materials of MNs, etc, and as such, it is necessary to choose the MNs for specific application as well as the target tissue.²⁷⁻

32

In addressing these points in this paper, MNs have been used to enhance the penetration depths of low density micro-particles (dry particulates) using an experimental set up that mimic particle accelerator (e.g. gene guns) in its operation principle. As model particles, we use biomedical grade stainless steel micro-particles. Further, a ground slide is used to prevent the impact of high pressure gas on the micro-particle target as discussed in more detail in the next section. The use of the ground slide gives lower particle velocities compared with the CST under the same operating conditions, which aims to reduce the cell damage. However, the purpose of the micro-particle gun is to accelerate the particles to a sufficient velocity which can penetrate into a desired depth inside the target. For a MN based injection system, this objective could be achieved by first applying solid MNs as they help in overcoming the tissue barrier.³³⁻³⁵ In this study, solid MNs are used to create well defined holes in the target which remain open immediately after removing the MN. Hence, a number of micro-particles should penetrate into the target via the holes to achieve the purpose of enhanced penetration depth. An increased penetration depth of micro-particles should allow deeper tissue to be transfected if DNA/genes are coated on the micro-particles. Therefore, the application of the MN based particle delivery is a good improvement for particle injectors.

In addition to the aims discussed above, this paper aims to investigate the significance of various important factors, e.g., the ground slide on the particle velocity for the MN assisted micro-particle injection. The micro-particles are mixed with PVP, compressed and bound as a cylindrical pellet for the purpose of this work. The pellet is mounted on a ground slide, which is accelerated along a barrel. The high velocity pellet is separated by a mesh which presents a partial blockage to the flow. The work in this paper aims to determine the passage

percentage and separated particle size. The paper also aims to study the effect of the MN on the micro-particle penetration depth when they are fired into a homogeneous agarose gel which is used as a model target. Agarose gel has the advantages that it can be produced with a controllable mechanical property and its transparency provides a good quality to view the micro-particle penetration using optical digital microscope. In agarose gel, the micro-particles follow two routes of delivery. The first route is that a number of micro-particles directly penetrate into the agarose gel without going through the holes created by MNs. The second route is that the micro-particles are delivered through the pierced holes created by the MNs to enhance the penetration depth inside the agarose gel. In reality, the target skin for these micro-particles may be different structurally and heterogeneous, and therefore the routes of the micro-particle delivery may be affected by its individual layers. However, this is not a consideration in this study as we carry out the experiments in a controlled manner using homogeneous agarose gels. The detailed information on the MN based injection system is described in section 2.2.

2. Material and Methodology

2.1 Materials

Biocompatible stainless steel micro-particles of high sphericity equalling approximately to 0.92 were bought from LPW Technology Ltd (Daresbury, UK). Detailed characterizations of these micro-particles are presented in section 2.3.2. Polyvinylpyrrolidone (PVP) purchased from Sigma-Aldrich Company Ltd. (Gillingham, UK) was dissolved in ethanol (analytical grade, 99%, obtained from Fisher Scientific Ltd., Loughborough, UK) and used to bind the micro-particles to form a cohesive mixture which could be compressed into a pellet. Agarose powder (Sigma-Aldrich Company Ltd., Gillingham, UK) was used to prepare an agarose gel which was used as a target for the micro-particles penetration experiments.

Photoelectric sensors (PS) were purchased from SICK Group (Waldkirch, Germany) to detect velocity of the micro-particles pellets loaded onto a ground slide. Meshes of three different pore sizes were obtained from Streme Limited (Marlow, UK). A solid MN array (Adminpatch) which has 31 needles of 1500 μm length was purchased from nanoBioSciences Limited Liability Company (LLC)(Sunnyvale, CA, USA).

2.2 Experimental design

In order to study the micro-particle delivery process, an experimental rig was constructed as shown in Fig. 1. Detailed information of the relevant parts of the experimental rig is listed in Table 1. The micro-particle transfer process in such systems can be divided into three stages: acceleration, separation and deceleration stage. For the acceleration stage, the pellet of micro-particles attached to ground slide is accelerated to a desired speed by a pressurized gas which was air in this study. The ground slide blocks the direct flow of gas out of the barrel and high pressure gas is released through a venthole, avoiding impact and gas damage on the skin, agarose gel or any other target of the micro-particles. Thus, there is no gas flow in the separation and deceleration stages. In the separation stage, the pellet is released from the ground slide after hitting a stopping wall. The pellet is released from the ground slide, hits a mesh placed at the end of the barrel which then breaks into a dispersion of micro-particles by high speed impaction on an open mesh. For the deceleration stage, the separated micro-particle spray forward, penetrate into the target via holes created by MNs and stop inside the target.

The detailed operating principle of the experimental rig is described as follows: a regulator is used to control the maximum gas pressure released from the gas cylinder. A control valve is located between the gas cylinder and receiver to manipulate the gas flow from the cylinder and store it in the receiver for the experiment. Additionally, a pressure transducer (PT-1) (Druck Ltd., Leicester, UK) is placed after the control valve to measure the pressure inside the receiver. A solenoid valve is used to operate the gas release from the receiver. It can open and close the gate according to a predetermined time and control the amount of gas released as required.

For the experiments, the barrel is mounted horizontally. A second pressure transducer (PT-2) (Druck Ltd., Leicester, UK) is located at the start of the barrel to detect the driving gas pressure for accelerating the ground slide. This is because a large pressure drop occurs between the receiver and the barrel due to the solenoid valve and the converging section of the receiver. It means that the pressure inside the receiver is not the same as the driving pressure for ground slide acceleration. The ground slide loaded with a pellet is placed at the start of the barrel. Two photoelectric sensors are located at the end of the barrel, which are separated by a distance of 25 mm. They are connected to an oscilloscope to record the relevant signals and measure the velocity of the ground slide. The principle of the

measurement of the ground slide speed is described in the section 2.3.1. In addition, two ventholes are made at the end of the barrel for release of the pressurized gas. Additionally, a mesh is placed into a muzzle at the end of the barrel and is held in place by a mesh holder. A test tube is also mounted in a holder placed at the end of the barrel to collect the separated particles and to determine the particle passage percentage (some particles remained trapped on the mesh and some rebound into the barrel). The detailed method is explained in section 2.3.2. In order to investigate the effect of MN indentation on the micro-particle penetration, the test tube is filled with agarose gel. The pellet is fired into this agarose gel to analyze the MN effects on particle delivery.

2.3 Methods

2.3.1 Experimental data acquisition

The detection of the ground slide velocity

The velocity of the ground slide was detected by a pair of photoelectric sensors. The photoelectric sensors consist of a light source (SICK Group, Waldkirch, Germany) and receiver (SICK Group, Waldkirch, Germany), and they are connected to an oscilloscope to record the relevant electrical signals. Two photoelectric sensors were located within the barrel, which are marked as PS-1 and PS-2 in Fig. 1. The barrel was made of stainless steel, and the inside surface was polished smooth to reduce friction. The space between the two photoelectric sensors is set at 25 mm. The working principle in this case is that the oscilloscope starts to record the signal after the ground slide reaches the position of the first sensor and covers the laser light. After the ground slide passes the second sensor, the oscilloscope records the time for the ground slide to travel from the first sensor to the second one. Thereby, an average velocity for the speed of the ground slide was obtained based on the known distance and recorded time.

The analysis of the pellet separation

The micro-particles were compressed into the form of a cylindrical pellet for firing in the experimental rig. To make the pellet the main materials used were biomedical grade stainless steel particles, PVP and 99% ethanol. At this stage of the research no DNA or drug was loaded on the micro-particles. PVP powder dissolved in ethanol was used to bind the stainless steel particles together (acting as a glue-like substance) as it has been used as a binder in many other pharmaceutical pellets³. The reason for choosing ethanol is that it helps

to dry the pellet quickly due to its high volatility. The strength of the pellet is related to the PVP concentration and, as such the ethanol does not affect the binding strength of the pellet. In this study, five solutions of differing PVP concentrations were made, namely 40, 60, 75, 90 and 100 mg of PVP per ml of ethanol. Based on the porosity of the micro-particle pellets (37.6%) and the size of the pellet, the desired amount of the PVP solution was added to 0.035 g of stainless steel powder by micro-pipette to fill the void space. We allow this mixture to dry for 1 – 2 minutes approximately at room temperature. When it is almost dry we transform the powdered stainless steel with PVP solution into a solid cylindrical pellet by a pellet press (Fig. 2). As shown in the figure, the stainless steel pellet press consists of a cover, shim, main body, base, rod and two seals. The operating procedure of this pellet press is as follows. The main body is placed on top of the base and one of the seals is inserted into the holes of the main body. Then the powdered stainless steel micro-particles containing PVP solution are added followed by the second seal. The rod is placed into the cover and inserted into the main body after placing the shim on the top of main body. Finally, the top cover is pressed until there is no space between the shim and the cover. Uniformly sized of pellet can be pushed out slowly using the rod directly into the ground slide to hold the pellet.

In the separation stage, the pellet is separated by a mesh and fired into an empty test tube. However, some of the separated particles are unable to pass through the mesh due to the blockage of the mesh. The analysis of the pellet separation is mainly focused on studying the passage percentage and the size of the separated particle. The mass of the pellet and test tube are measured before the experiment. The mass of the collected particles is obtained after measuring the mass of the test tube after firing. The passage percentage is calculated as:

$$\text{Passage percentage} = \frac{t_1 - t_2}{m} \times 100 \quad (1)$$

where t_1 is the mass of the test tube after firing and t_2 is the mass of the test tube before firing, m is the initial mass of the pellet.

In addition, the separated particle sizes should be considered carefully to determine if any large agglomerates remained which could affect the performance of the system and penetration depth and damage to the target area. For this measurement, an adhesive-coated

tape is placed at the end of the rig instead of the test tube (Fig. 1). The pellet is directly fired into the tape through the mesh, where the particles get stuck. The particle laden adhesive-coated tape is then analyzed in detail by scanning electron microscope (SEM).

2.3.2 Characterization of the micro-particle

Fig. 3 shows a SEM image of the stainless steel micro-particles before they are made into a pellet form in this study. As can be seen, most of the particles range between diameters of 1 to 20 μm , although a few larger diameter particles were found to be present. Majority of the micro-particle was less than 15 μm in diameter. From the SEM images, 30 randomly selected particles were analyzed further to calculate the average sphericity of the micro-particle sample which is found to be 0.92 ± 0.05 . The actual density of the micro-particles and the bulk density of the pellet without PVP are $\sim 8 \text{ g/cm}^3$ and $4.98 \pm 0.02 \text{ g/cm}^3$, respectively. The porosity of the pellet without PVP is found to be $37.6 \pm 0.3 \%$ from equation (2)

$$\text{Porosity} = 1 - \frac{\rho_{\text{bulk}}}{\rho_{\text{particle}}} \quad (2)$$

Where ρ_{bulk} is the bulk density of the pellet and ρ_{particle} is the density of the particle material. In the experiment, we measure the volume of the pellet and the mass of the micro-particles to obtain the bulk density which are then used to calculate the porosity of the pellet using the equation above. The pellet has negligible amount of PVP mass and it is assumed it does not affect the bulk density or the porosity of the pellet. The ethanol that is used to dilute the PVP evaporates off from the pellet and therefore it does not affect the pellet porosity.

2.3.3 Characterization of the MN

A MN patch (Adminpatch 1500) which has 31 MNs on a 1 cm^2 circular patch was used. As shown in Fig. 4, the MNs are distributed as a diamond array on the patch. The space between two MNs on the side direction is 1546 μm . The spacings between two MNs on the two diagonal directions are 1970 and 3000 μm . The length, thickness and width of each MNs are 1500, 78 and 480 μm , respectively.

2.3.4 Characterization of the mesh

Stainless steel woven meshes were chosen in this case due to their strength, higher open area and their acceptance in pharmaceutical research. Three different mesh sizes were used in this study for pellet breakage, which are explained more in Table 2. As shown in the table,

the mesh pore size decreases with an increase in mesh size. The wire diameter also has an effect on the pore size and to some extent on the fractional open area. However, for the meshes used here the fractional open area remains approximately the same, which allows for easier comparison of the results for the different pore sizes.

3 Results and Discussions

As stated earlier, the micro-particles delivery process can be divided into three stages, namely, acceleration, separation and deceleration. In the following sections the results corresponding to each of these stages are presented and discussed.

3.1 Particle acceleration stage

3.1.1 The velocity measurement of the ground slide

Some of the key variables of importance in this study are the operating pressure, the barrel diameter and length, and their effects on the velocity of the ground slide. The pellet velocity is also of importance which is equal to the ground slide velocity at the end of the barrel. The operating pressure of the receiver (Fig. 1) is another major factor that affects the velocity of the ground slide. In the developed rig, a significant pressure drop occurs after the release of gas from the receiver due to a converging area of the receiver and losses in a solenoid valve attached to the receiver. Therefore, the pressure inside the receiver is not the actual pressure that accelerates the ground slide. The pressure at the start of the barrel is directly measured by a pressure transducer (PT-2), as explained in the section 2.2. The pressure inside the gas receiver ranges from 10 to 40 bar while the actual pressure to accelerate the ground slide varies between 3 to 6 bar as measured by the pressure transducer, i.e. there is about 70 - 85 % pressure drop for the system as the gas is released from the receiver. As shown in Fig. 5, the velocity of the PTFE ground slide shows a positive correlation with the actual acceleration pressure. The particle velocity can achieve a maximum of 102, 123, 139 and 148 m/s at 3, 4.5, 5.5 and 6 bar pressures for the longest barrel. Fig. 5 shows a significant difference in velocity between the two different lengths of barrel; longer barrels allow a greater time for acceleration of the ground slide. For both barrels, the velocity increases at a low rate at higher pressure. The effect of pressure on the velocity of the ground slide decreases gradually, because of (i) increased friction and (ii) the length of barrel is fixed, so the time for acceleration is reduced, even though the acceleration rate itself increases.

In this study, PTFE and stainless steel ground slides have been prepared to investigate how the material density affects the ground slide acceleration. The mass of the ground slide for each material made is listed in Table 3 in detail. As shown in Fig. 6, the velocity of the ground slide is very different for the PTFE and stainless steel materials at the same operating condition. The density of the material affects the mass of the ground slide, making it more difficult to accelerate; hence increased ground slide density has a negative effect on the acceleration. Similarly, Fig. 6 shows that an increase of the barrel diameter causes a decrease on ground slide velocity. The mass of the ground slide increases as the barrel diameter is increased.

Overall, it is obvious that the mass of the ground slide is important in the acceleration stage. As expected, the mass increases as the barrel diameter is increased. It also increases with an increase in the material density and ground slide length. On the other hand, the velocity of the ground slide decreases with the increase in its mass. These suggest that a narrow diameter should be used for such studies as it reduces not only the ground slide diameter but also its mass.

Based on the above results (Fig. 5 and 6), a barrel with 8 mm diameter and 500 mm length and PTFE ground slide (12.5 mm long) were chosen for the following study on the particle separation stage. The velocity of solid PTFE ground slide is 148 m/s at 6 bar pressure. The micro-particles can achieve the speed over of 600 m/s at much higher pressure for a CST, e.g., at 60 bar^{13,16}. This is because the effect of the ground slide is to reduce the effect of the fired micro-particles. Mitchell et al.¹³ have used a LGG¹⁴ which loaded the micro-particles in a ground slide that the effect of the ground slide is investigated. It obtained that the; their particle velocity is slow downies were reduced to 170, 250, 330 m/s at 2, 4 and 6 MPa pressure. However, the pressure drop that occurs in our system means that all micro-particles are accelerated to the same extent for a given barrel length. Therefore, an increased acceleration distance (barrel length) which makes up for the pressure drop effect for the current system has been chosen. Finally, the particle velocity for the current system is shown to be slightly different from that in the LGG¹⁴ operated at 20 bar pressure. As a result, the particle velocity is slower if compared with the velocity obtained for other types of gene gun, largely due to the pressure drop effect. A decreased velocity decreases the micro-particle penetration due to a reduction of particle momentum. However, the application of a solid MN

patch has promised to remove this disadvantage since the pierced holes remain in the target tissue when the MN patch is removed and a number of micro-particles can then reach further depths via the pierced holes. This is explained more in the section 3.3.

3.2 Particle separation stage

The analysis of the pellet separation for MN based injection system is described below. The passage percentage was analyzed in relation to the known pellet separation variables of operating pressure, PVP concentration and mesh pore size. In addition, the micro-particles size resulting from the separation stage was studied using scanning electron microscope.

3.2.1 Effect of the operation pressure

Pellet was made using between 40 and 60 mg/ml PVP (pellet binder) concentration and results were obtained for operation between 2.4 to 4.5 bar pressures and for mesh with pore sizes of 310 and 178 μm . As shown in Fig. 7, with increasing pressure (and hence increasing velocity) the passage percentage increases rapidly at low pressures and then remains approximately constant. This is because the velocities of the pellets are larger under higher operating pressures, which cause the separated particles to gain more momentum before they are disrupted by passage through the mesh. The results show a significant increase in passage percentage from 2.4 to 3.5 bar followed by much slower increase from 3.5 to 4.5 bar. This means that at lower operating pressures there is a greater effect of pressure on the passage percentage. It is likely that the passage percentage reaches a maximum and then decreases due to some particles sticking to the mesh and some rebounding, hence not passing into the test tube (particle collector). At lower pressure conditions, the impact force on the mesh is smaller and hence the pellet is not broken up as effectively, sometime forming larger aggregates of particles, which block the mesh pores. Therefore, a larger amount of the separated particles were unable to pass through the mesh. Fig. 7 also shows the passage percentage increases with an increase of mesh pore size and a decrease of PVP concentration. The detailed effects of the PVP concentration and pore size on passage percentage are explained in the following sections.

3.2.2 Effect of PVP concentration

In general, the binding strength of the pellet increases with an increase in the PVP concentration, which in turn causes the passage percentage to decrease. The effect is

however quite weak, as shown in Fig. 8 which suggests that the passage percentage only gradually decreases with an increase of PVP concentration. The fall in passage percentage with increasing PVP concentration is due to the greater adhesive forces and increased strength of pellet, which are present in the higher PVP concentrations. The larger particles or agglomerates, i.e. those which are greater in size than the mesh opening, are unable to break up as the PVP concentration increases which means that they cannot pass through the mesh. Instinctively, the effect of PVP concentration on passage percentage should be lower at higher operating pressure. This is because the impact force on the mesh is larger causing the pellet to separate more easily. However Fig. 8 shows that the range of binder concentrations used here does not lead to a significant change in the percentage of the pellet which passes through the mesh.

3.2.3 Effect of the mesh pore size

The effect of the mesh pore size on the pellet separation is one of the main variables that affect the particle separation. This is because the pore size is able to affect the size of the separated particles that pass through the mesh. This characteristic of the mesh could also affect the passage percentage, e.g. by blocking if the smallest mesh pores. To investigate the effect on the pellet separation, three different pore size meshes are studied at a constant pressure of 4.5 bar. The detailed information is explained in the Table 2, which shows that although the pore size changes, the fractional open area remains approximately constant for these meshes.

Fig. 9 shows that the passage percentage exhibits significant differences for the various mesh pore sizes. As expected, the passage percentage has positive correlation with the pore size; larger pore sizes allow larger separated particles to pass through. In addition, the PVP concentration represented a negative effect on passage percentage especially for the smallest pore size mesh. The mesh with the largest pore size (about 310 μm) allowed the highest passage percentage of particles to pass through for each PVP concentration. In contrast, the mesh with the lowest pore size of 122 μm yielded the lowest passage percent. The next section discusses the effects of pore size and PVP concentration of the size distribution of the separated particles.

3.2.4 The analysis of the separated particle size

To achieve the desired particle delivery, one of the factors that are crucial to control is the size distribution of the separated micro-particles. In general, the mesh pore size is able to manage the size distribution of the separated particle as it prevents passage of large particles. In this study, three different meshes were used at pressure of 4.5 bar in order to find out the effects of mesh pore size on the separated particles. The detailed information on the meshes is shown in Table 2. Fig. 10a shows an SEM of the particles produced by the mesh with pore size 122 μm ; the pellet has been efficiently broken into individual particles with only a few small agglomerated particles. The maximum size of the agglomerated particle is about 50 μm . As expected, this mesh resulted in a lower passage percentage compared to the results of the other two meshes. The passage percentage improved for the mesh with pore size 178 μm (as shown in Fig. 9) and the resulting separated particles are shown in Fig. 10b. This mesh also broke the pellet into individual particles and prevented passage of large sized agglomerates. The maximum size of the separated agglomerates is about 70 μm . The application of the mesh with pore size 310 μm gave the maximum passage percentage. However, as Fig. 10c indicates some large agglomerated particles remain; the size of the largest agglomerate goes up to about 175 μm .

Overall, it can be concluded from this section that the size of the separated particles is controlled by the mesh pore size. The two smaller pore sizes resulted in effective pellet separation into individual particles, with relatively few large agglomerates.

The PVP concentration is also a major factor in determining the size distribution of the separated particles as it provides a binder which affects the strength of the pellet and binds the particles. Four different PVP concentrations were used to make the pellets which were fired at a pressure of 4.5 bar and mesh with pore size 178 μm . Fig. 11a shows the separated particles for 40 mg/ml PVP concentration. As can be seen, the pellet was efficiently broken up into individual particles with only a few small agglomerated particles. The passage percentage decreased only slightly after increasing the PVP concentration to 60 mg/ml for the pellet and the resulting particles are shown in Fig. 11b. A number of agglomerates were observed at this condition. As shown in Fig. 9, the passage percentages are not significantly different for different PVP concentrations between 60 to 90 mg/ml. Fig. 11b-d shows that some agglomerated particles were able to pass through pores of the 178 μm mesh. However, a 40 mg/ml PVP concentration made pellet provides a good control on the size distribution of the

separated particle and a higher passage percentage, i.e. it has sufficient binder strength to form the pellet that can be manipulated and mounted on the ground slide, but not so much strength that it affects particle separation.

The results show that size distribution of the separated particle tends to be narrow for the smaller mesh pore size. Meshes with pore size 122 and 178 μm displayed a good quality of the size distribution for 40 mg/ml PVP concentration made of pellet. In addition, a mesh with a pore size of 178 μm yields a higher passage percentage. Large separated particles can significantly damage the target tissue are detrimental and hence are not acceptable in this study. In addition, the strength of the pellet also does not allow the particles delivery due to a lack of particle separation. Most of the pellets should be separated into individual micro-particles, and the maximum agglomerated particle size should be kept below a target of 70 μm .

3.3 Deceleration stage

3.3.1 The micro-particle penetration in agarose gel

An aqueous gel made using 0.02 g/ml agarose was chosen as a target medium to study the effect of the solid MN application on the micro-particle penetration. The gel is a homogenous and transparent material, which provides a good measure of the micro-particle penetration. In the experiment, agarose powder is dissolved into water and heated in a microwave heater which is then added into a sliced test tube. The test tube is covered solidly from one side with a removable film. Thus, a flat surface of agarose gel is obtained after the removal of the film when the gel is set in the test tube. The MN array is manually pressed by putting a flat plate on the back of the MN array which provides a uniform force to pierce the MN into the gel until the backing surface of the MN just contacts the gel surface. This flat surface is used as an object of reference for the determining the insertion of the MNs. Also it is used for the measurement of the particle penetration depth. Fig. 12 shows a typical distribution of the stainless steel micro-particles after impact on surface of the agarose gel. As can be seen, the micro-particles were non-uniformly distributed of the gel, with a maximum concentration at the centre coinciding with the impact position of the pellet on the mesh. In this experiment, the MN array (see Fig. 4) had been pressed into the surface of the gel and then removed. The holes created by the MN array are clearly visible and they remain on surface of the agarose gel. The size and shape of these holes change only very slowly with time after the MNs are

withdrawn. The agarose gel is a viscoelastic material like skin and the MN holes therein shrink with time. We have used 10 holes to obtain an average length of the pierced holes in the agarose gel which is found to be approximately 720 μm when Admipatch MN 1500 is inserted.

In order to determine the micro-particle penetration, agarose gel was cut into thin slices (approx. 1 mm thick) by razor sharp blades and analyzed in more detail using a digital optical microscope (Eclipse 3100 & Digital Sight, Nikon). As shown in Fig. 13, the holes were formed and remained in the gel after the application of the solid MN. Fig. 13 also shows that the stainless steel micro-particles were visible in the gel surface and within the holes. As can be seen, the micro-particles seem to have a larger penetration depth compared to those that have not entered through the pierced holes on the left side of the figure. As expected, the micro-particles can penetrate into a deep area via the holes. The other micro-particles only have a little penetration without the hole. The maximum penetration depths are shown in Table 4 in detail.

As discussed before, Mitchell et al.¹³ used a LGG to accelerate 99 μm diameter polystyrene micro-particles and achieved a maximum penetration depth of 150 μm at 60 bar pressure. Kendal et al.³⁶ used a convergent-divergent device to accelerate gold particles of diameter 1.8 μm which achieved a maximum penetration depth of 78.6 μm at 60 bar. As can be seen from Table 4, the maximum penetration depth in this study seems to improve in comparison of the results of Mitchell et al.¹³ and Kendal et al.³⁶. However, an agarose gel of concentration 0.02 g/ml may not mimic the human skin properties exactly and as such, the implication of the mechanical properties of the target should be analyzed in more detail. Nevertheless, the results in this paper show that the application of a solid MN has a beneficial effect on the micro-particle penetration depth. In addition, the agarose gel provides a good condition for the measurement of the micro-particle penetration depth by a digital optical microscope. A skin mimicking agarose gel will be considered in another study to demonstrate further that MN based system has a positive effect for micro-particle delivery and the implications of the mechanical properties of the target tissue.

4 Conclusions

An experimental rig involving a micro-particle delivery and injection system has been built in this study to determine if solid MNs can enhance the penetration depths of the low density micro-particles which may be used to deliver genes and drugs. For the purpose of this design, the micro-particle delivery process has been separated into three stages. For the first stage, namely, the acceleration stage, the results show that an increase in the mass of the ground slide which carries the particles in the form of a pellet causes a negative effect on the ground slide acceleration and hence a reduced velocity of the micro-carrier pellet. The mass of the ground slide is related to its material density and size where the size is typically determined by the barrel diameter. Based on the present result, a narrow barrel was chosen for the study of the separation and deceleration stages as it has positive effect on the mass of the ground slide and pressure drop. For the separation stage, the passage percentage was measured using an empty test tube to collect the separated stainless steel particles which had been broken by passage through a mesh. The results show that the passage percentage increases with pressure and mesh pore size but decreases with increasing pellet binder concentration. Increased binder concentration causes an increase of pellet strength, which seems to have a negative effect on the pellet separation. The mesh pore size affected the break up of the pellets into individual particles; larger mesh sizes allowed large agglomerated particles to pass through, which is not desirable. The mesh pore size has a significant effect on the size distribution of the separated particle and it can separate the pellet properly into individual particles. In addition, higher binder concentration pellets led to an increased number of large agglomerated particles. This is not desirable because the large particles can significantly damage the target tissue. Pellets bound with 40 mg/ml PVP yielded a higher passage percentage and a good control on the size distribution of separated particle based on the application of 178 μm pore size mesh. For the deceleration stage, 2% concentration of agarose gel was chosen as a transparent target material to study the effect of solid MN application on micro-particle delivery. The results show the pellet is well separated and sprayed onto the target; a number of stainless steel micro-particles can penetrate a deep area inside the gel due to the holes created by the solid MN application. The maximum penetration depth is comparable with previous study^{13,36} and in some cases shows a significant improvement, but without the need for high pressure gas flows which can damage soft tissues. However this should be investigated further in a future study.

5 Acknowledgement

Loughborough University (UK) is acknowledged for providing a PhD studentship to Dongwei Zhang which made this work possible. Further, the technical supports from Mr Tony Eyre, Mr Mark Barron, Mr Jim Muddimer, Mr Terry Neale and Mr Steve Bowler are gratefully acknowledged.

6 Reference

1. Klein T.M., Wolf E.D., Wu R. and Sanford J.C., (1987). High-velocity microprojectiles for delivering nucleic acids into living cells, *Nature*, **327**:70-73
2. Heiser W.C., (1994). Gene transfer into mammalian cells by particle bombardment, *Analytical Biochemistry*, **217**(2): 185-196
3. Svarovsky S., Borovkov A., Sykes K., (2008). Cationic gold microparticles for biolistic delivery of nucleic acids, *Biotechniques*, **45**(5): 535-540
4. Huang P.H., Chen P.Y., (2011). Design of a two-stage electromagnetic impulse force circuit for gene gun, *Journal of Marine Science and Technology*, **19**(6): 686-692
5. O'Brien J.A., Lummis S.C.R., (2011). Nano-biolistics: a method of biolistic transfection of cells and tissues using a gene gun with novel nanometer-sized projectiles, *BMC biotechnology*, **11**: 66
6. Manjila S.B., Baby J.N., Bijin E.N., Constantine I., Pramod K., Valsalakumari J., (2013). Novel gene delivery system, *International Journal of Pharmaceutical Investigation*, **3**(1):1-7
7. Dempster A.C. Topham S.J., Johnson M.J., Hickey P.L., Longridge D.J., (2000). Comparison of epidermal thickness to skin response in various species following systemic drug delivery using a dermal PowderJet particle delivery system, *J Pharm Pharmacol*, **52**: 49
8. Kendall M.A.F., (2002). The delivery of particulate vaccines and drugs to human skin with a practical hand-held shock tube-based system, *Shock Wave*, **12**: 23-30
9. Bellhouse B.J., Sarphe D.F., and Greenford J.C., (1994). Needleless syringe using supersonic gas flow for particle delivery, *Int.PatentWO94/24263*
10. Burkoth T.J., Bellhouse B.J., Hewson .G, Longridg eD.J., Muddle A.G., Sarphe D.F., (1999). Transdermal and transmucosal powdered drug delivery, *Crit. Rev. Drug Carrier System*, **16**(4):331-84

11. Quinlan N.J., Kendall M.A.F., Bellhouse B.J., Ainsworth R.W., (2001). Investigations of gas and particle dynamics in first generation needle-free drug delivery device, *Shock Waves*, **10**:395-404
12. Kendall M.A.F., Quinlan N.J., Thorpe S.J., Bellhouse B.J., Ainsworth R.W. (2004). Measurements of the gas and particle flow within a converging-diverging nozzle for high speed powdered vaccine and drug delivery, *Exp. Fluids*, **37**: 128-36
13. Mitchell T.J., Kendall M.A.F., Bellhouse B.J., (2003). A ballistic study of micro-particle penetration to the oral mucosa, *International Journal of Impact Engineering*, **28**:581-99
14. Crozier W.D., Hume W., (1957). High velocity light gas gun, *Journal of Applied Physics*, **28**(8): 892-895
15. Liu Y., Truong N.K., Kendall M.A.F., (2004). Numerical studies of contoured shock tube for murine powdered vaccine delivery system, 15th Australasian Fluid Mechanics conference.
16. Liu Y., and Kendall M.A.F., (2006). Numerical analysis of gas and micro-particle interactions in a hand-held shock-tube device, *Biomed Microdevices*, **8**:341-51
17. Soliman S.M., Abdallah S., Gutmark E., Turner M.G., (2011). Numerical simulation of miroparticles penetration and gas dynamics in an axi-symmetric supersonic nozzle for genetic vaccination, *Powder Technol.*,**208**:676-83
18. Belyantseva I A., (2009). Helios gene gun-mediated transfection of the inner ear sensory epithelium, *Methods MolBiol*, **493**: 103-124.
19. Xia J.X., Martinez A., Daniell H., Ebert S.N., (2011). Evaluation of biolistic gene transfer methods in vivo using non-invasive bioluminescent imaging techniques, *BMC Biotechnology*, **11**: 62
20. Uchida M., Li X.W., Mertens P., Alpar H.O., (2009). Transfection by particle bombardment: Delivery of plasmid DNA into mammalian cells using gene gun, *Biochim. Biophys. Acta.*, **1790**(8):754-764
21. Trainer A.T., Alexander M.Y., (1997). Gene delivery to the epidermis, *Human Molecular Genetics*, **6**(10): 1761 - 1767
22. Henry, S., McAllister, D.V., Allen, M.G., Prausnitz, M.R., (1998). Microfabricated MNs: a novel approach to transdermal drug delivery. *J. Pharm. Sci.*, **87**: 922-925.
23. Prausnitz M.R., (2004). MNs for transdermal drug delivery. *Advanced drug delivery reviews*. **56**: 581–587.

24. Al-Qallaf, B and Das, DB (2009). Optimizing microneedle arrays for transdermal drug delivery: Extension to non-square distribution of microneedles, *Journal of Drug Targeting*, 17(2), 108-122.
25. Ashraf, M.W., Tayyaba, S., Afzulpurkar, N., (2011). Micro electromechanical systems (MEMS) based microfluidic devices for biomedical applications. *Int. J. Mol Sci.* 12:3648-3704.
26. Nayak, A and Das, DB (2013). Potential of biodegradable microneedles as a transdermal delivery vehicle for lidocaine, *Biotechnology Letters*, (in press). DOI; 10.1007/s10529-013-1217-3
27. Olatunji et al, 2013. Olatunji, O, Das, DB, Garland, MJ, Belaid L, Donnelly, RF, *Journal of Pharmaceutical Sciences*, 102(4), 1209–1221, April, DOI: 10.1002/jps.23439
28. Olatunji, O, Das, DB, Nassehi, V. 2012. Modelling transdermal drug delivery using microneedles: Effect of geometry on drug transport behaviour. *Journal of Pharmaceutical Sciences*, 101(1), 164–175, January, DOI: 10.1002/jps.22736.
29. Yan G., Warner K. S., Zhang J., Sharma S., Gale B. K., (2010), Evaluation needle length and density of microneedle arrays in the pretreatment of skin for transdermal drug delivery, *International journal of Pharmaceutics*. **391**: 7-12.
30. Donnelly R.F., Raj S.T.R., Woolfson A.D., (2010). Microneedle-based drug delivery systems: microfabrication, drug delivery, and safety, *Drug Deliv.*, **17**(4): 187-207
31. Al-Qallaf, B, Das, DB, Davidson, A (2009). Transdermal drug delivery by coated microneedles: geometry effects on drug concentration in blood, *Asia-Pacific Journal of Chemical Engineering*, 4(6), 845–857, November/December, DOI: 10.1002/apj.353.
32. Teo A.L., Shearwood C., Ng K.C., Lu J., Moochhala S., (2006). Transdermal microneedles for drug delivery applications, *Materials Science and Engineering*, **132**: 151-154.
33. Chu L.Y., Choi S.O., Prausnitz M.R., (2010). Fabrication of dissolving polymer MNs for controlled drug encapsulation and delivery: Bubble and pedestal MN designs, *J Pharm. Sci.* **99**(10): 4228-4238
34. Coulman S., Allender C., Birchall J., (2006). MNs and other physical methods for overcoming the stratum corneum barrier for cutaneous gene therapy, *Ther. Drug Carrier Syst.* **23**(3): 205-258

35. Stahl J., Wohlerl M., Kietzmann M., (2012). MN pretreatment enhances the percutaneous permeation of hydrophilic compounds with high melting points, *BMC Pharmacology and Toxicology*, **13**: 1-7
36. Kendall M.A.F., Rishworth S., Carter F., Mitchell T., (2004). Effects of relative humidity and ambient temperature on the ballistic delivery of micro-particles to excised porcine skin, *J. Invest. Dermatol.* **122**: 739-746

List of Tables

Table 1: The equipments and important parameter values for the experiment

Table 2: Important properties of the meshes

Table 3: The key variables effect on the mass of the ground slide

Table 4: The penetration depths of the micro-particles

Table 1: The equipments and important parameter values for the experiment

Part name	Important variable	Material/Chemical/other component
Gas cylinder	Initial pressure: 200 bar Size: 146cm×23cm Mass: 82kg	Compressed air Supplier: BOC (UK)
Regulator	Pressure range: 0-300bar	Supplier: WIKA Instruments Limited (Redhill, UK)
Control valve	Pressure range: 0 – 100 bar	Supplier: Swagelok Company (Solon, USA)
Pressure transducer	Range : 0 -100 bar Type: XML-G100D71	Supplier: Druck Ltd. (Leicester, UK)
Receiver	Volume:1 L	Supplier: HOKE Inc.(Spartanburg, USA)
Solenoid valve	Pressure range: 0 – 100 bar	Supplier:Connexion developments Ltd(Yate, UK)
Timer	Range: 0.1 – 12 sec Type: H3DE-F	Supplier: OMRON Electronics Ltd (Milton Keynes, UK)
Ground slide	Diameter: 8 mm/15mm Length: 12.5 mm	PTFE
Pellet	Diameter: 2 mm Length: 2 mm	Stainless steel micro-particle
Barrel	Diameter: 8mm/15mm Length: 500 mm/250mm	Stainless Steel
Venthole	Diameter: 4 mm	n/a
Muzzle	Hole diameter: 3 mm	Stainless Steel
Mesh holder	n/a	Stainless Steel
Test tube holder	n/a	PTFE
Oscilloscope	Type: TDS 3034B	Supplier: Tektronix (Sweden, UK)
PS	Response time: 16μs Scanning range up to 20m Type: WLL180T	Supplier: SICK Group (Waldkirch, Germany)

Table 2: Important properties of the meshes

Mesh size	Pore size (μm)	Wire diameter (μm)	Open area (%)
50	310	0.20	37%
80	178	0.14	31%
120	122	0.09	33%

Table 3: The key variables effect on the mass of the ground slide

Material	Diameter(mm)	Length(mm)	Density(g/cm ³)	Mass(g)
PTFE	8	12.5	2.2	1.3
PTFE	15	12.5	2.2	4.85
Stainless steel	8	12.5	8.0	4.6
Stainless steel	15	12.5	8.0	17.7

Table 4: The penetration depths of the micro-particles

PVP concentration (mg/ml)	Pressure (bar)	Maximum Penetration depth with hole (μm)	Penetration depth without hole (μm)
40	4.5	515.7 \pm 124.3	221.4 \pm 44.8
	3	508.6 \pm 137.2	118.7 \pm 20.3

List of Figures

Fig. 1: Schematic diagram of the experimental rig

Fig. 2: Schematic diagram of the pellet press

Fig. 3: SEM image of the stainless steel micro-particles

Fig. 4: Adminpatch 1500 microneedle array

Fig. 5: The velocity of solid polytetrafluoroethylene(PTFE)ground slide against the operating pressure of gas receiver for different lengths of barrel

Fig. 6: The comparison of the effect of material on ground slide acceleration in the wide and narrow barrel for two different diameters of barrel/ground slide

Fig. 7: The effect of operating pressure on the passage percentage for two different PVP concentrations

Fig. 8: The PVP concentration effect on the particle passage percentage at various pressures

Fig. 9: The particle passage percentage against PVP concentration for various mesh sizes

Fig. 10: SEM image of the separated particle size which is made of 40 mg/ml PVP concentration and operated at 4.5 bar pressure: (a): 122 μ m pore size (mesh size 120), (b) 178 μ m pore size (mesh 80), (c) 310 μ m pore size (mesh 50)

Fig. 11: SEM image of the separated particle size which is operated at 20 bar pressure and mesh with pore size 178 μ m: (a): 40 mg/ml PVP concentration made of pellet, (b): 60 mg/ml PVP concentration made of pellet, (c): 75 mg/ml PVP concentration made of pellet, (d): 90 mg/ml PVP concentration made of pellet

Fig. 12: An image of the micro-particle sprayed on an agarose gel

Fig. 13: Optical microscope image of stainless steel micro-particle penetration into agarose gel (40mg/ml PVP, 4.5 bar, Mesh with pore size 178 μ m)

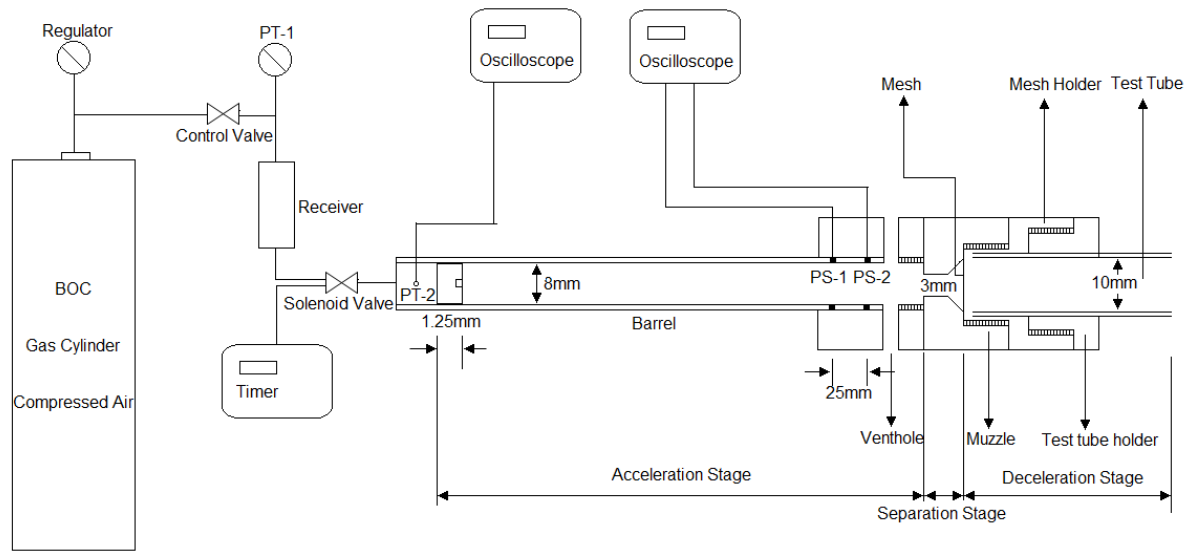
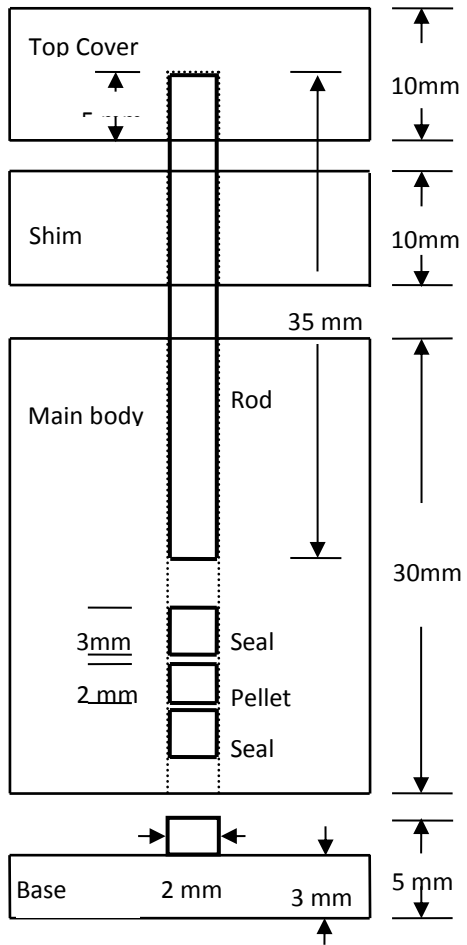


Fig. 1 Schematic diagram of the experimental rig



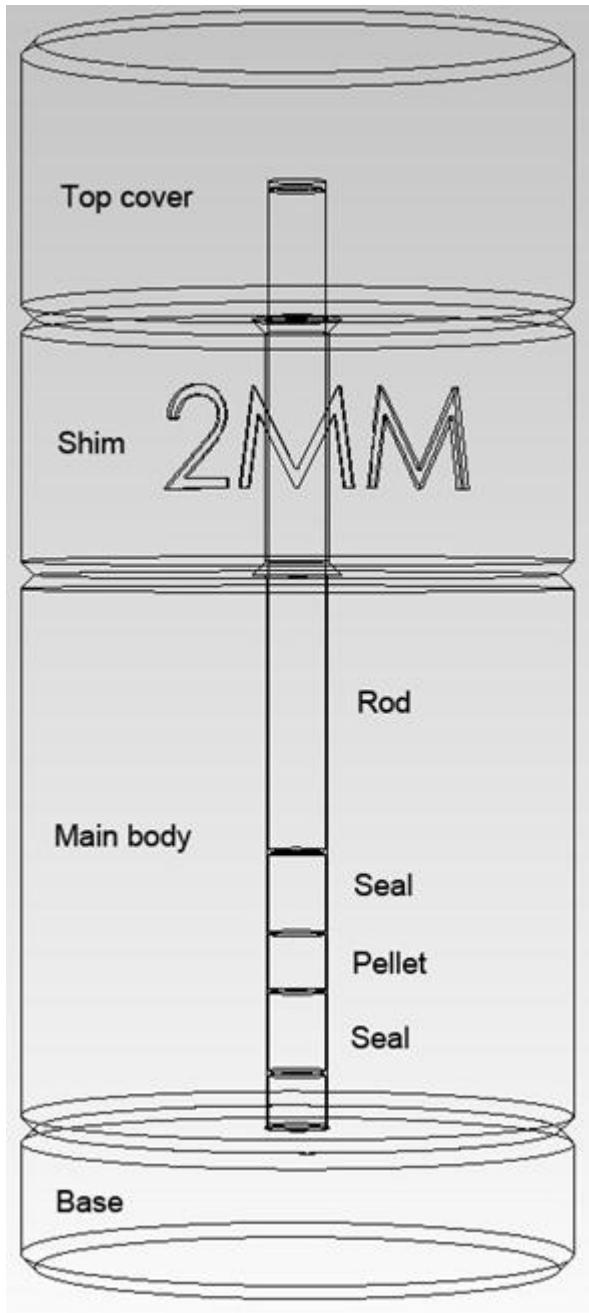


Fig. 2: Schematic diagram of the pellet press

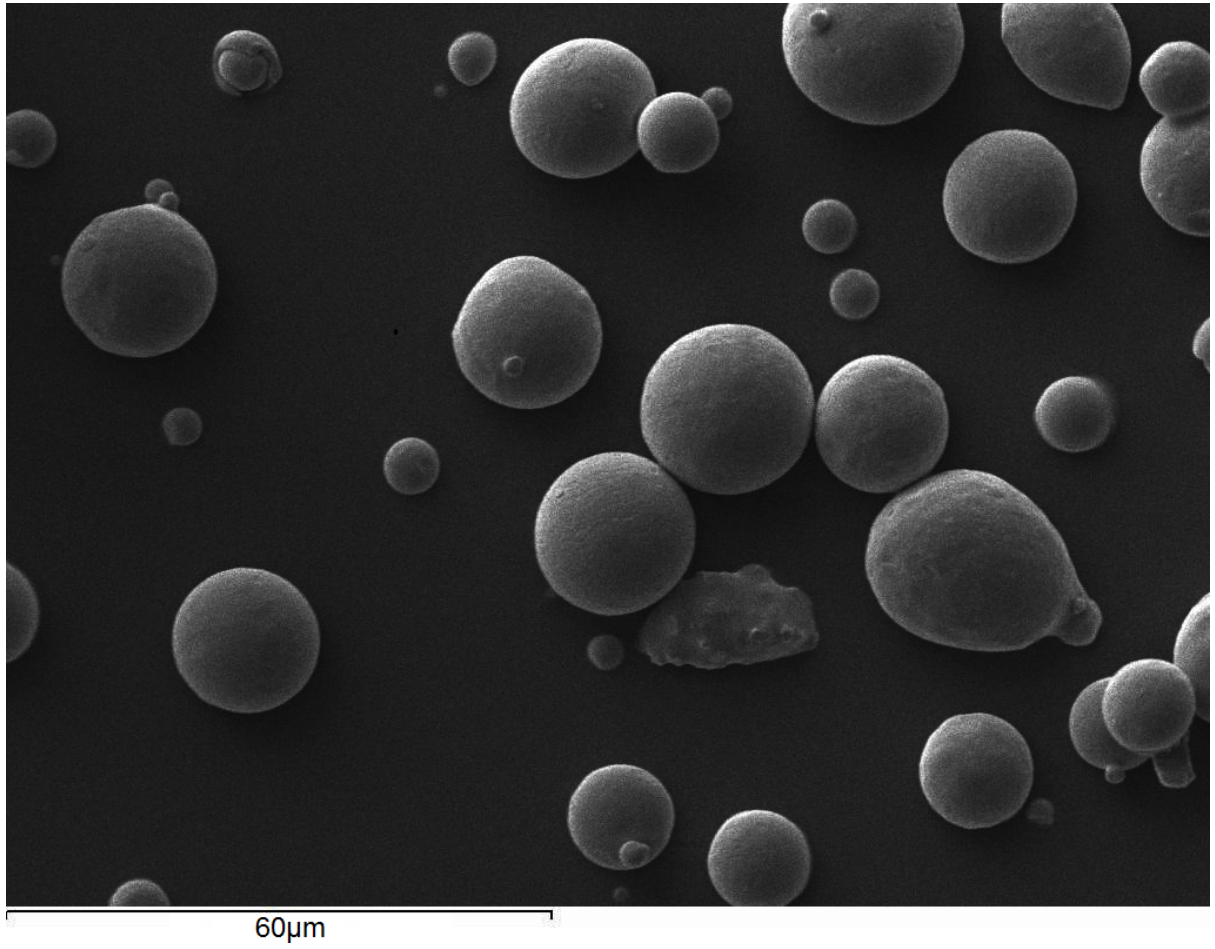


Fig. 3: SEM image of the stainless steel micro-particles

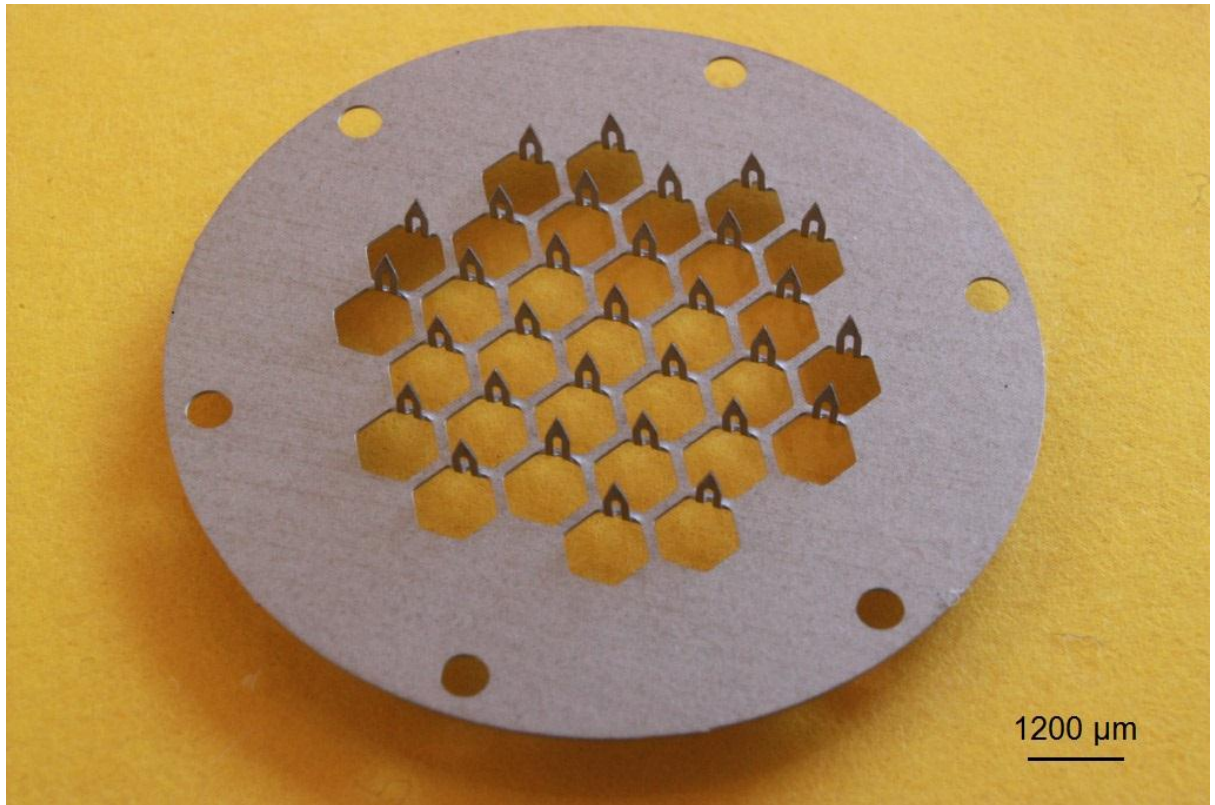


Fig. 4: Adminpatch 1500 microneedle array

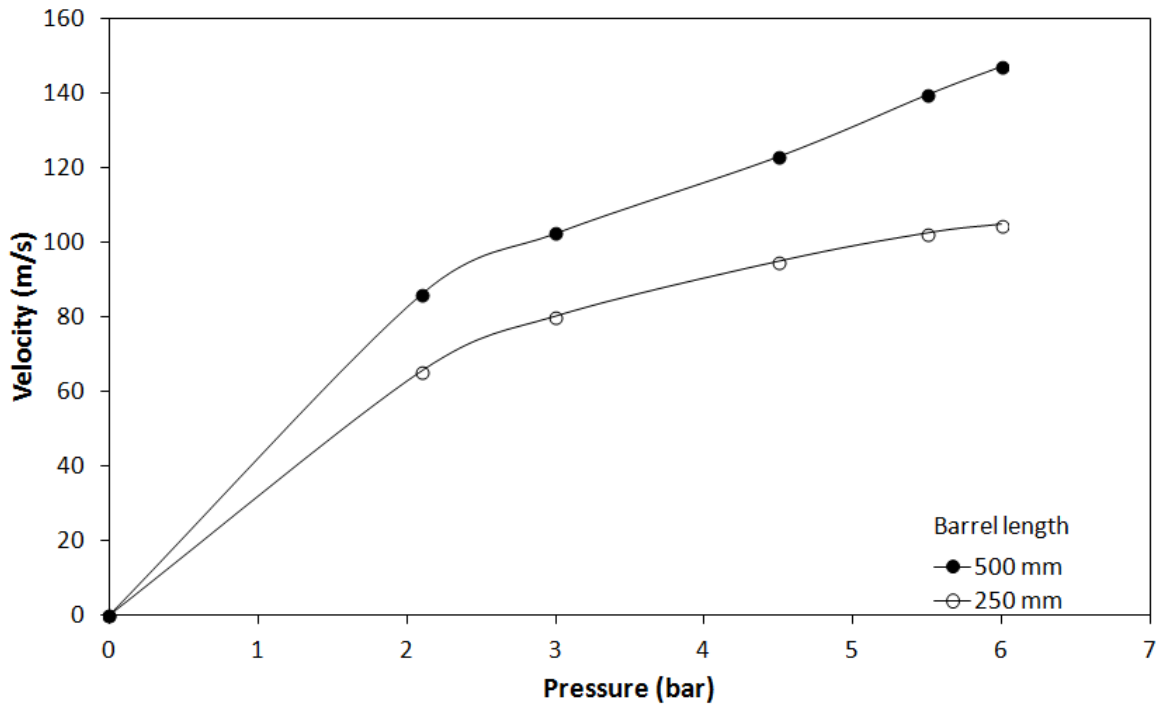


Fig. 5: The velocity of solid polytetrafluoroethylene (PTFE) ground slide against the operating pressure of gas receiver for different lengths of barrel (8 mm diameter)

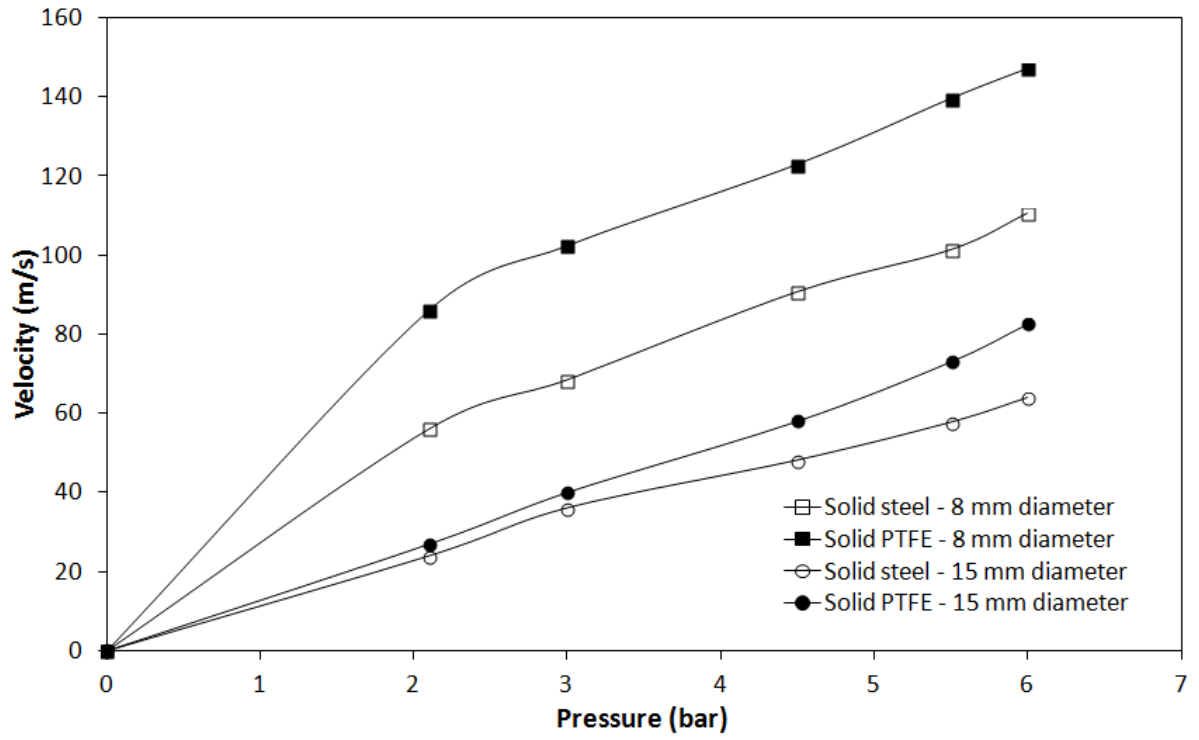


Fig. 6: The comparison of the effect of material on ground slide acceleration in the wide and narrow barrel for two different diameters of barrel/ground slide

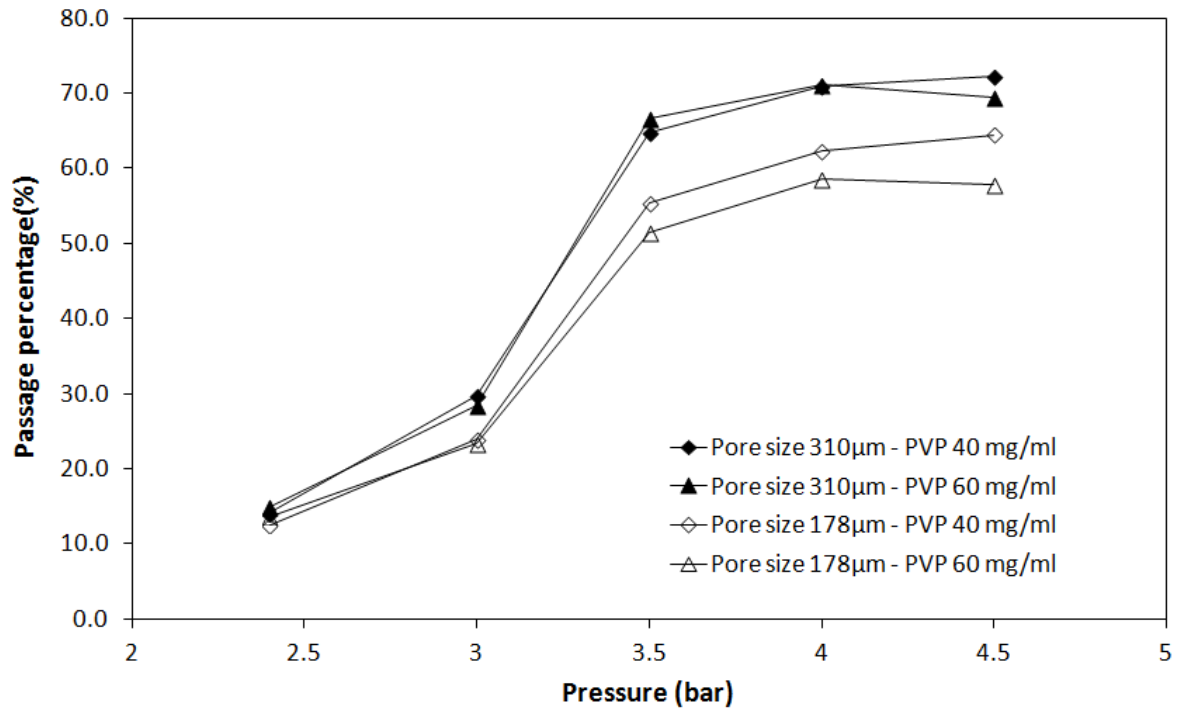


Fig. 7: The effect of operating pressure on the passage percentage for two different PVP concentrations

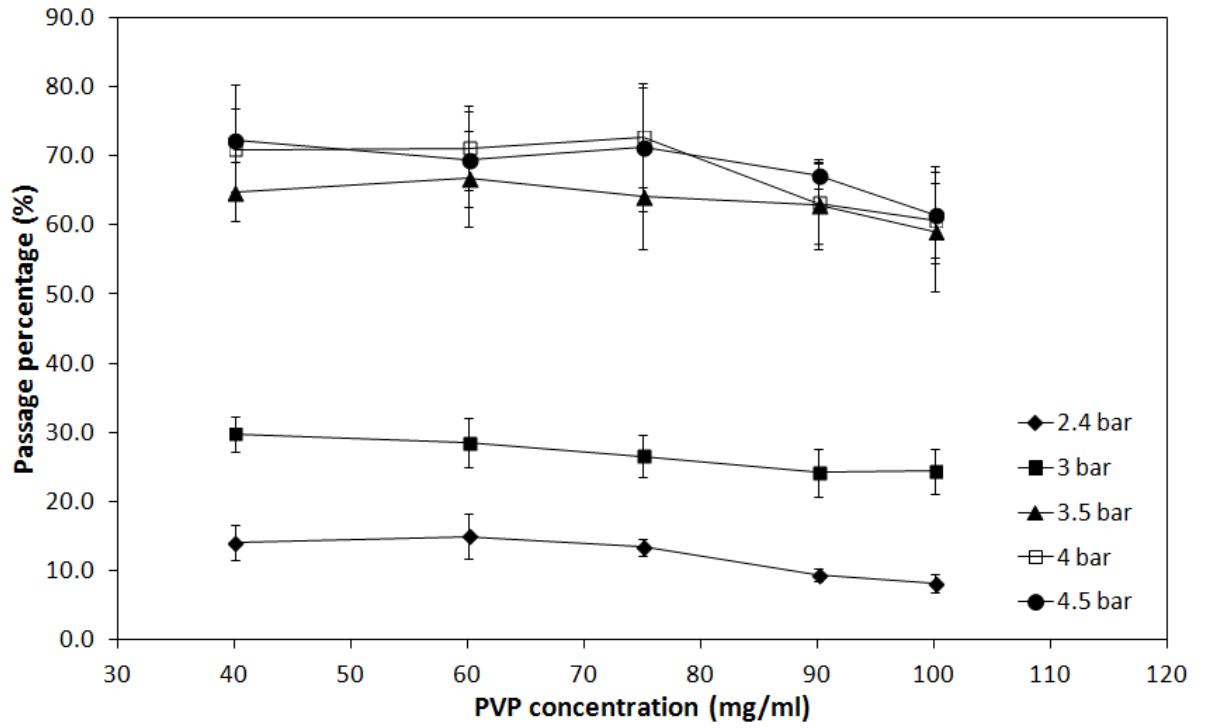


Fig. 8: The PVP concentration effect on the particle passage percentage at various pressures

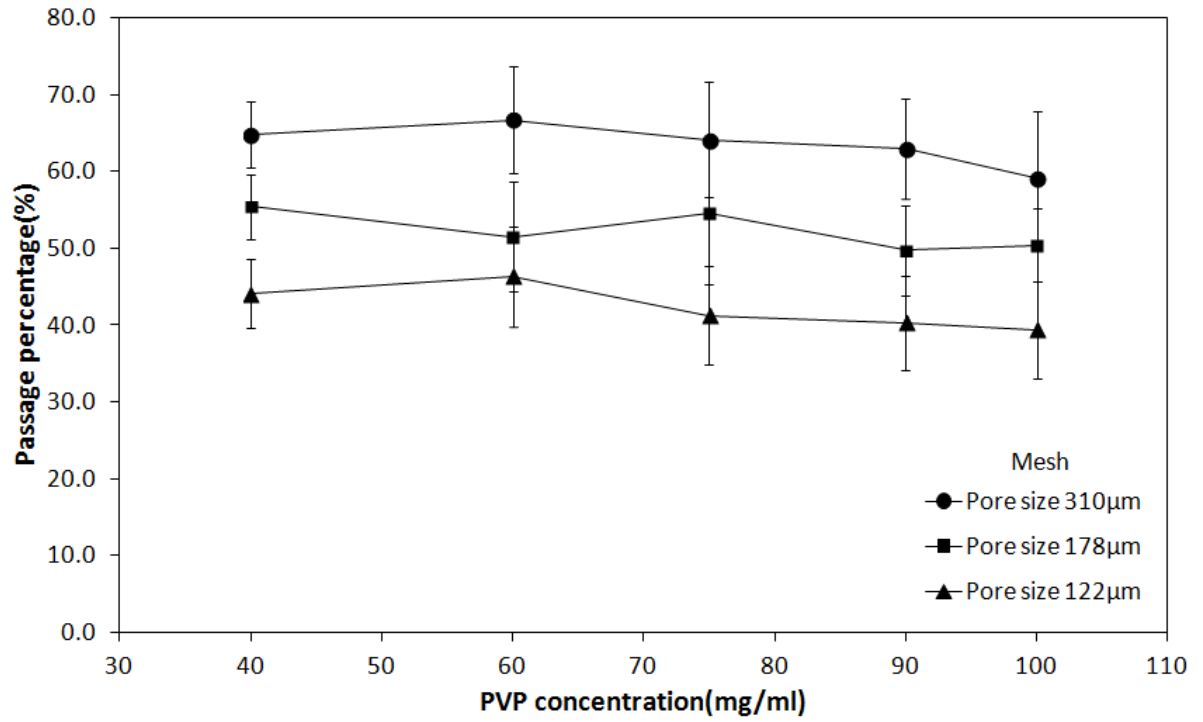
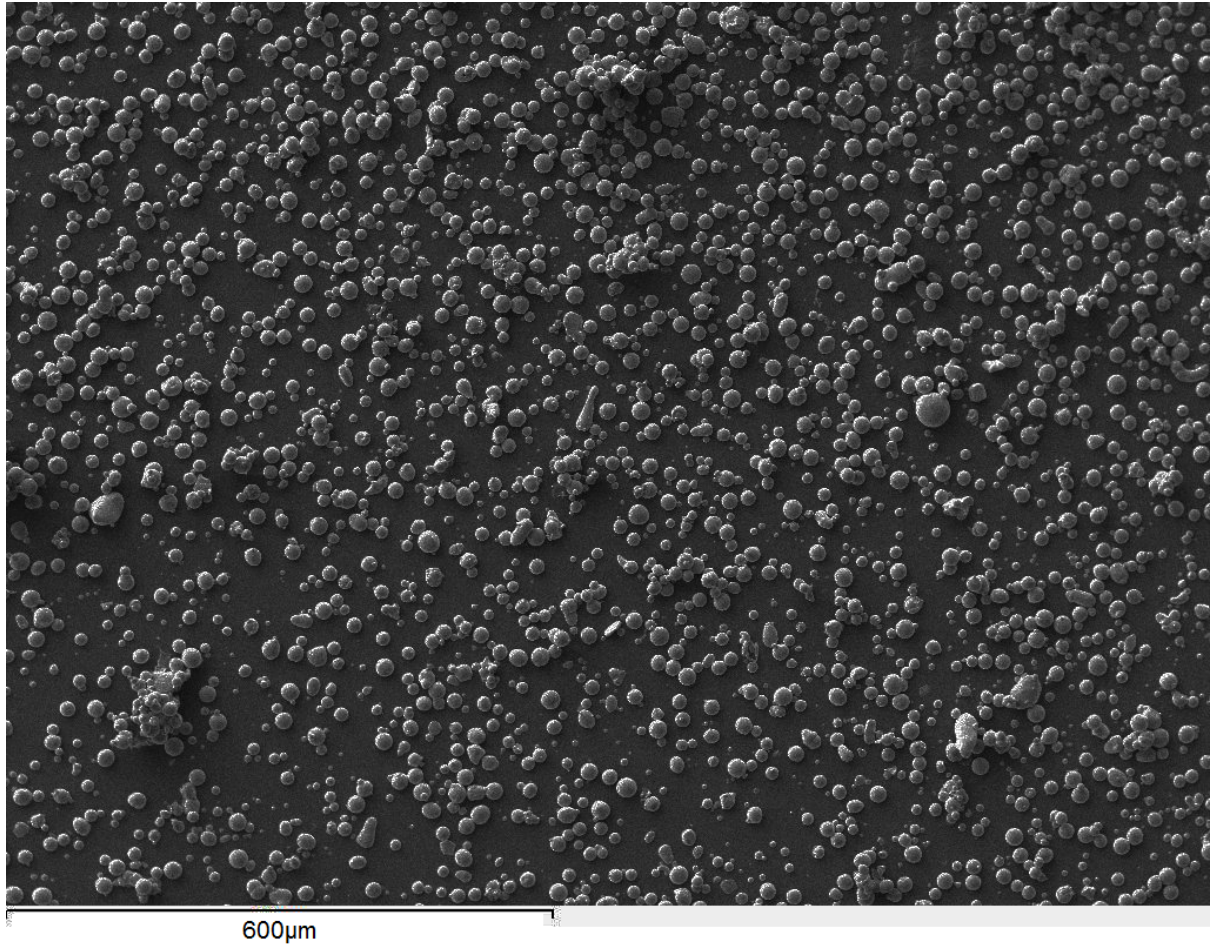
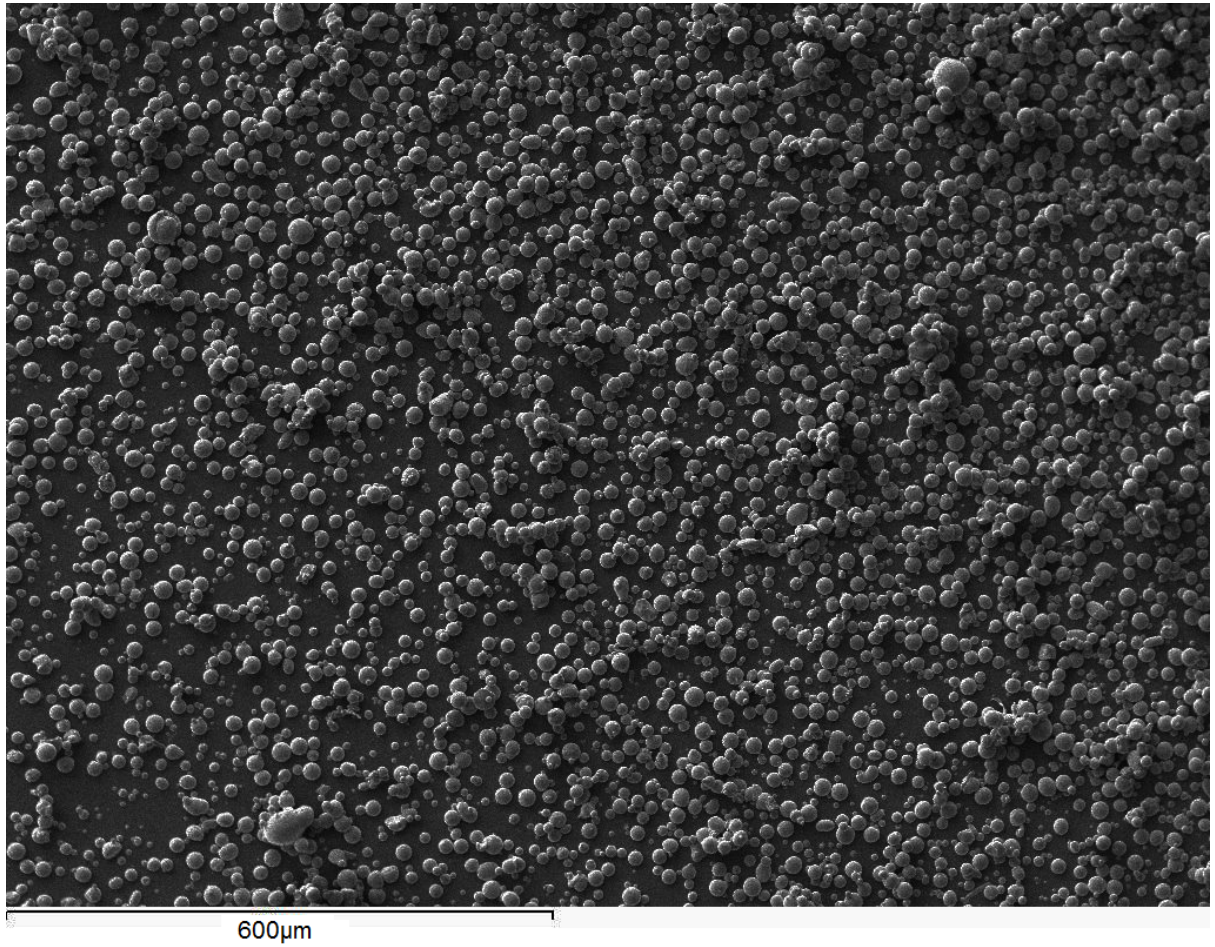


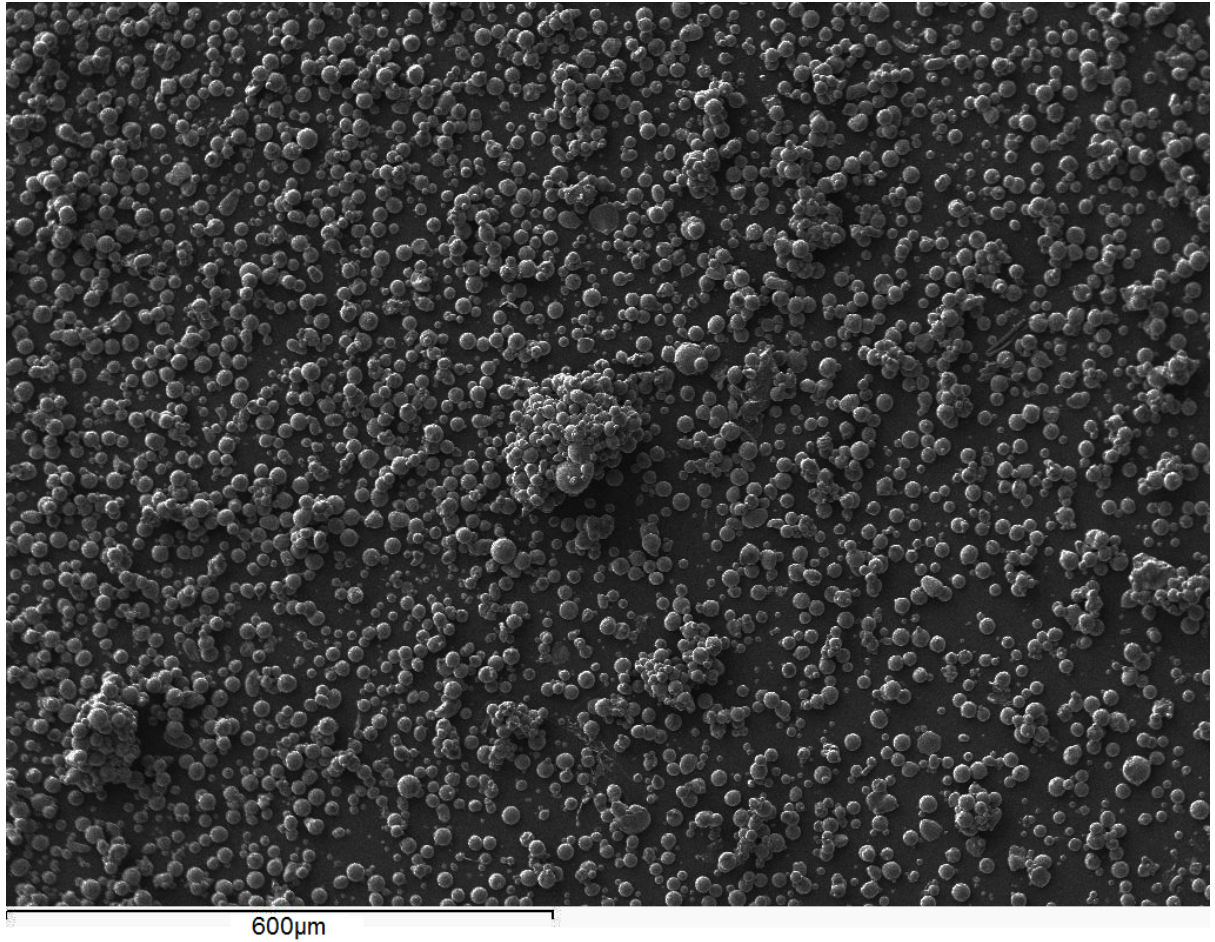
Fig. 9: The particle passage percentage against PVP concentration for various mesh sizes



(a): 122 μm pore size (mesh size 120)

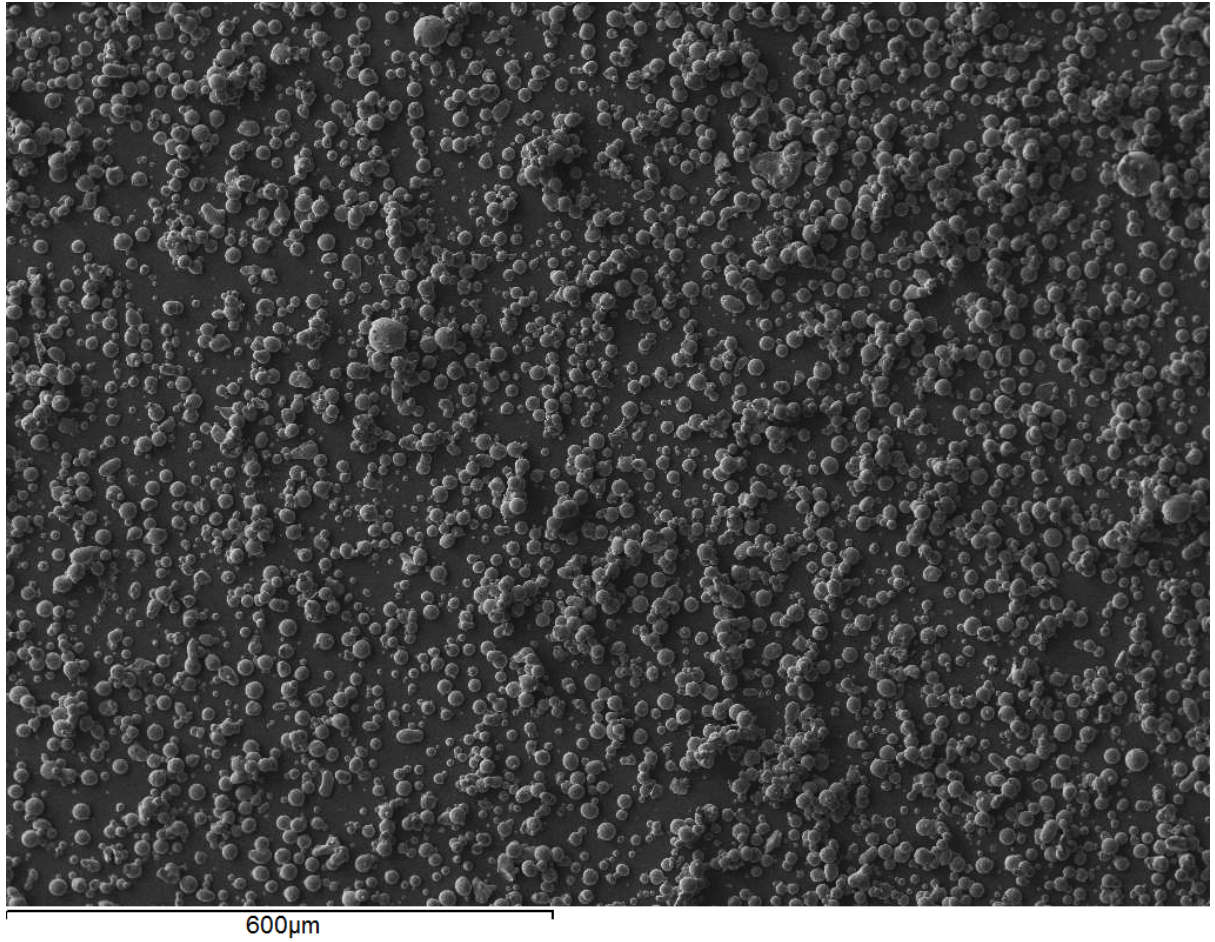


(b) 178 µm pore size (mesh 80)

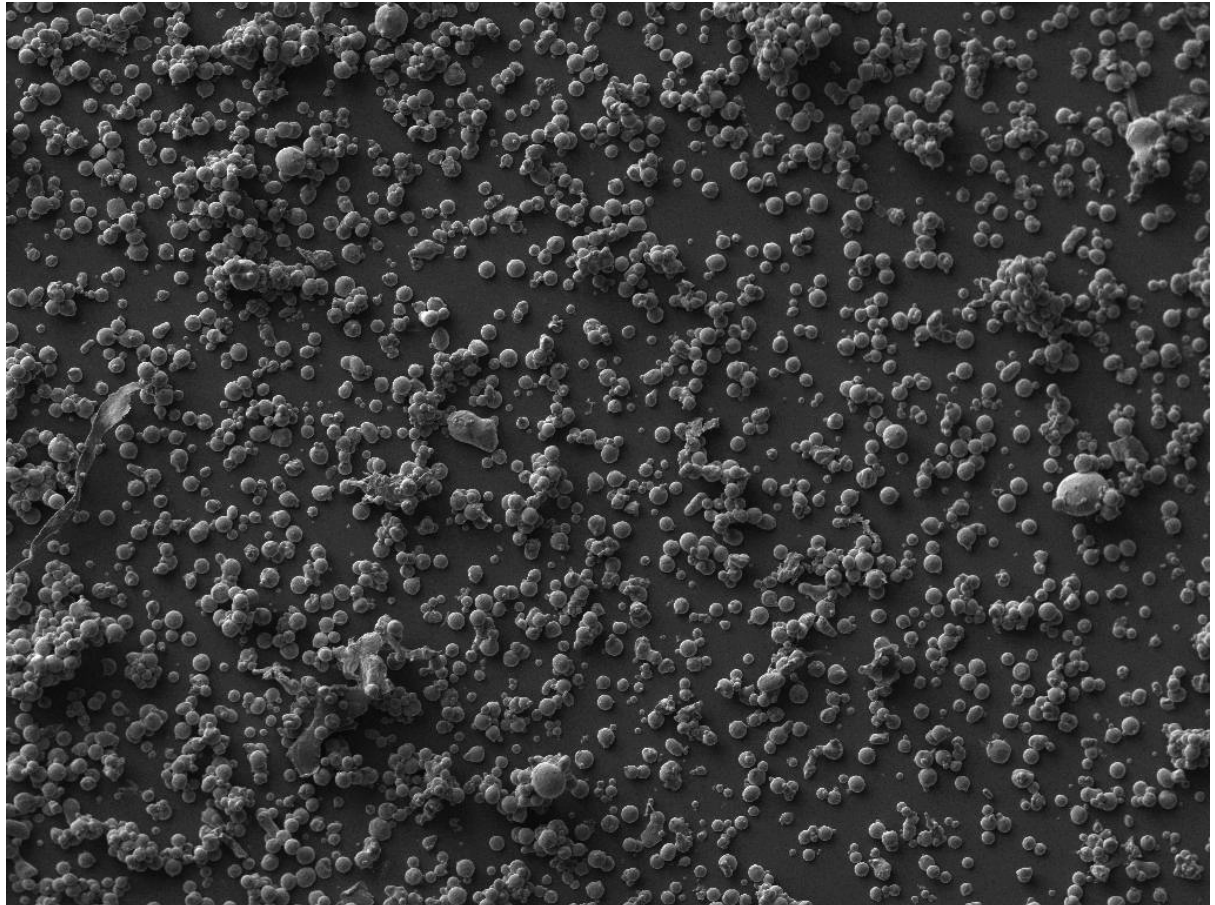


(c) 310µm pore size (mesh 50)

Fig. 10: SEM image of the separated particle size which is made of 40 mg/ml PVP concentration and operated at 4.5 bar pressure: (a): 122 µm pore size (mesh size 120), (b) 178 µm pore size (mesh 80), (c) 310 µm pore size (mesh 50)

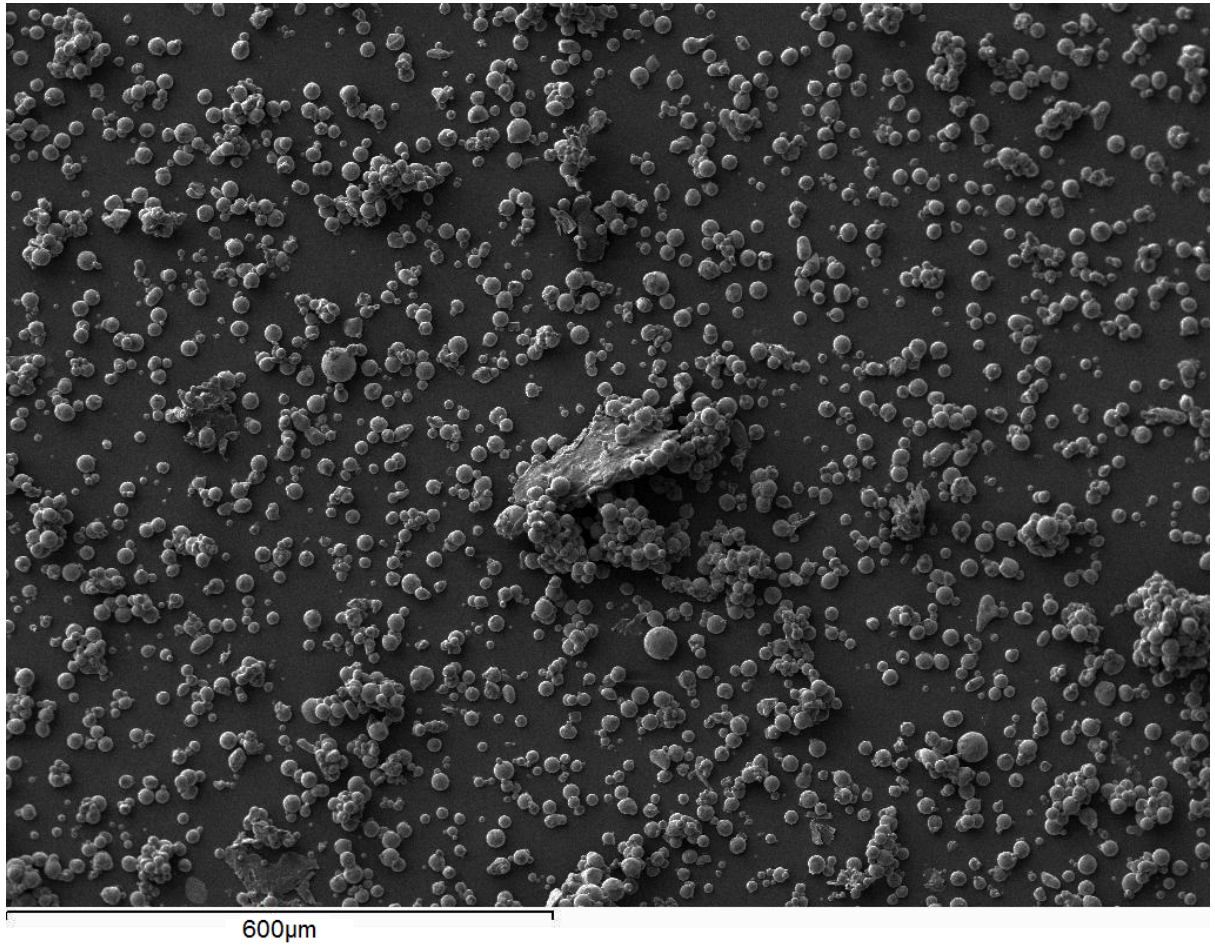


(a): 40 mg/ml PVP concentration made pellet

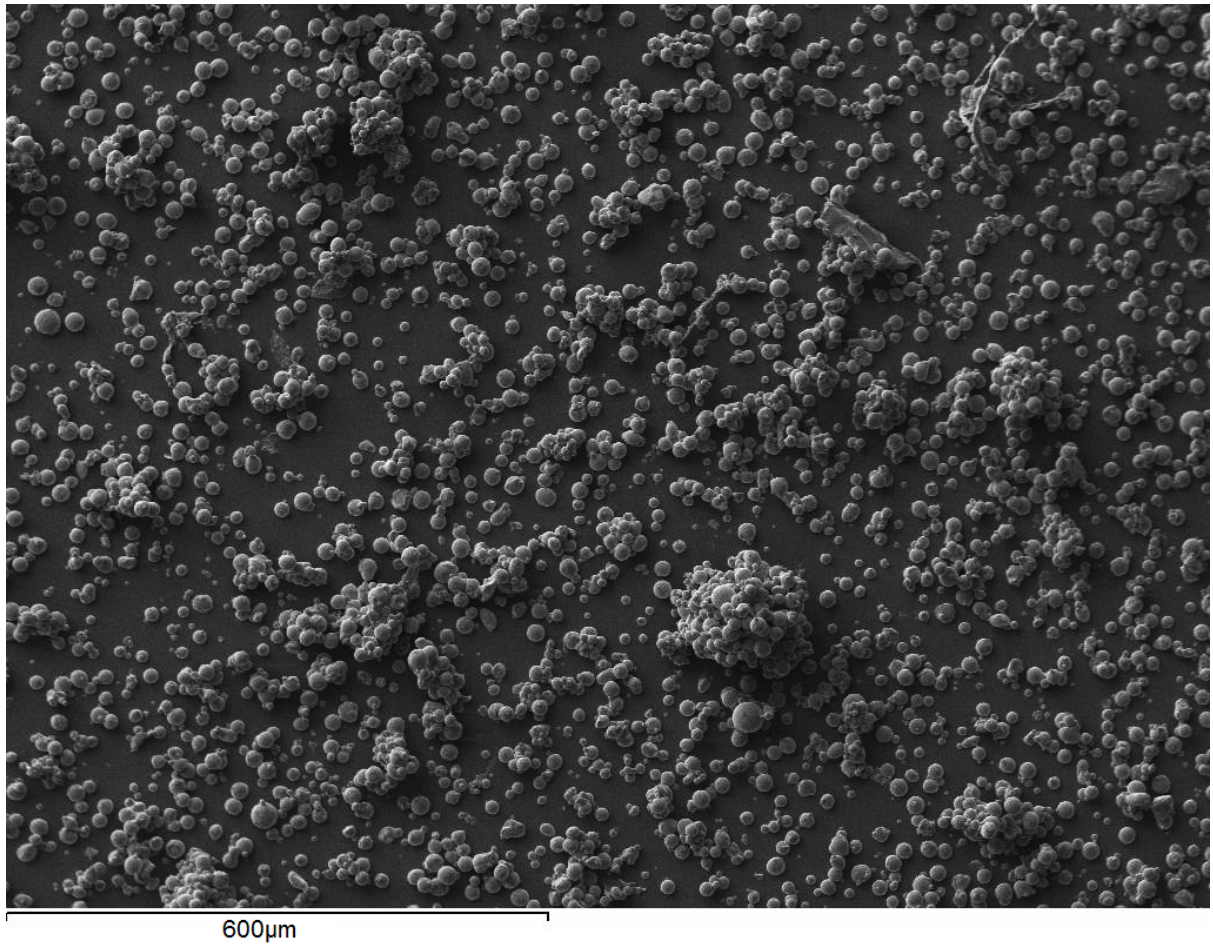


600µm

(b): 60 mg/ml PVP concentration made pellet



(c): 75 mg/ml PVP concentration made pellet



(c): 90 mg/ml PVP concentration made pellet

Fig. 11: SEM image of the separated particle size which is operated at 4.5 bar pressure and mesh with pore size 178 μm : (a): 40 mg/ml PVP concentration made pellet, (b): 60 mg/ml PVP concentration made of pellet, (c): 75 mg/ml PVP concentration made of pellet, (d): 90 mg/ml PVP concentration made pellet



Fig. 12: An image of the micro-particle sprayed on an agarose gel

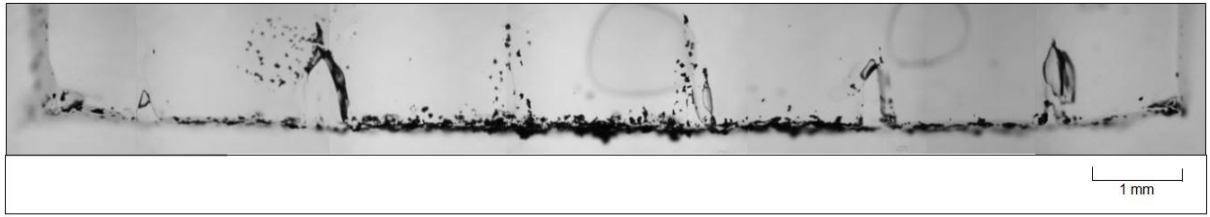


Fig. 13: Optical microscope image of stainless steel micro-particle penetration into agarose gel (40 mg/ml PVP, 4.5 bar, Mesh with pore size 178 μm)